Contact inhibition of locomotion generates collective cell migration without chemoattractants in an open domain

Hamid Khataee,[1,*] Andras Czirok,[2,3] and Zoltan Neufeld[1]
[1]*School of Mathematics and Physics, The University of Queensland, St. Lucia, Brisbane, QLD 4072, Australia*
[2]*Department of Biological Physics, Eotvos University, Budapest, 1053, Hungary*
[3]*Department of Anatomy and Cell Biology, University of Kansas Medical Center, Kansas City, Kansas 66160, USA*

(Received 15 December 2020; revised 20 March 2021; accepted 15 June 2021; published 12 July 2021)

Neural crest cells are embryonic stem cells that migrate throughout embryos and, at different target locations, give rise to the formation of a variety of tissues and organs. The directional migration of the neural crest cells is experimentally described using a process referred to as contact inhibition of locomotion, by which cells redirect their movement upon the cell–cell contacts. However, it is unclear how the migration alignment is affected by the motility properties of the cells. Here, we theoretically model the migration alignment as a function of the motility dynamics and interaction of the cells in an open domain with a channel geometry. The results indicate that by increasing the influx rate of the cells into the domain a transition takes place from random movement to an organized collective migration, where the migration alignment is maximized and the migration time is minimized. This phase transition demonstrates that the cells can migrate efficiently over long distances without any external chemoattractant information about the direction of migration just based on local interactions with each other. The analysis of the dependence of this transition on the characteristic properties of cellular motility shows that the cell density determines the coordination of collective migration whether the migration domain is open or closed. In the open domain, this density is determined by a feedback mechanism between the flux and order parameter, which characterises the alignment of collective migration. The model also demonstrates that the coattraction mechanism proposed earlier is not necessary for collective migration and a constant flux of cells moving into the channel is sufficient to produce directed movement over arbitrary long distances.

DOI: 10.1103/PhysRevE.104.014405

I. INTRODUCTION

Neural crest cells are motile embryonic cells which are present in all vertebrates and produce a variety of derivatives including neurons, pigment cells of the skin, cartilage, bone, muscle, and connective tissues of the skull, face, neck, and heart [1–4]. Following the formation of neural crest cells during vertebrate embryogenesis, the cells undergo an epithelial-to-mesenchymal transition which enables them to migrate long distances along specific pathways to different target locations throughout the embryo, where they differentiate into various essential cell types [1,4,5]. Due to this widespread contribution of neural crest cells to nearly every major organ, these cells serve as an important model system to study the physiological and pathological processes, e.g., birth defects and invasive cancers; reviewed in Ref. [6].

The migration of neural crest cell populations is a prime representation of the collective migration of a loosely associated stream of cells, because their migration as a collective emerges from their occasional temporary interactions [7–12]. Both *in vivo* and *in vitro* experiments describe the directional migration of the neural crest cells using contact inhibition of locomotion (CIL) by which cells reshape and change their direction of movement upon the cell–cell contacts [13,14]. CIL is also found to enhance the collective chemotaxis of neural crest cells towards a chemoattractant, where the cell density promotes the cells chemotactic response [15,16]. In contrast, dispersed single cells are unable to move towards the chemoattractant [11,17]. This presents the crucial role that CIL plays in the migration of neural crest cells during health and disease [7,9]. For instance, the loss of CIL behavior contributes to the malignant invasion, where the malignant tumour cells spread to the healthy tissues [7]. This suggests that targeting the collective behavior of a cell population may be effective in controlling the associated diseases, e.g., cancer metastasis [18].

A major class of theoretical models for collective migration has been developed in the area of animal migration. These models capture the group-level migratory properties using simple interaction rules, e.g., local alignment, attraction, and repulsion [19–24]. In these models, animals are represented as point particles which interact via nonlocal rules, because they use sight to interact with other animals at a distance. In the context of the cell migration, however, the directionality of the migration relies on the localized information provided by direct physical contacts or chemical signals [25].

In addition, the motility of multiple diffusive species (subpopulations), where the motility of a total population of motile agents or particles represented as a system of interacting subpopulations, has been studied in on-lattice [26] and off-lattice [27] models. These models describe the distribution of particles in space and time using systems of partial differential equations. Such approaches can be useful in tracking

*Corresponding author: h.khataee@uq.edu.au

a subpopulation of cells within a larger population, e.g., the movement of neural crest cells along the developing intestine, where donor quail cells were grafted into a chick host [28].

To describe the collective behavior of neural crest cells, earlier theoretical models have used various computational techniques (e.g., agent-based and Potts models) and analytical methods (e.g., partial differential equations) [28–32]. We have developed a two-dimensional computational model for the migratory dynamics of neural crest cells driven by CIL [33]. We modeled cell shapes as closed contours and analyzed the alignment patterns of the migration in a closed domain as functions of the cell density and shape [33]. CIL and chemoattraction toward a secreted chemical molecule have been suggested by earlier computational models as key mechanisms to spontaneous collective migration [34–37]. Although experiments have provided evidence to support the presence of neural crest chemoattractants *in vivo* [11,38,39], it is well documented that neural crest cultured *in vitro* in the absence of any external chemoattractant exhibit directional collective migration [11,31,40]. Yet, it remains poorly understood how the transmission of alignment information through the cell–cell interactions can affect their collective movement in an open domain, depending on the influx rate of cells into the domain and their motility properties.

Here, we analyze the role of the alignment interactions among cells (equivalent to CIL [19,33]) in the collective migration of cells in an open domain with a channel geometry, in the absence of cell proliferation and chemotactic signals. The open channel geometry is more realistic for the migration of neural crest cells, compared with a closed domain, as it enables us to compare our theoretical results with experiments and other modeling studies. In addition, we consider the migration of a stationary, continuous stream of cells within a channel, where cells enter the channel at a constant rate, rather than than the migration of a finite cell cluster in a channel studied in Refs. [31,34]. Furthermore, we consider a simplified model based on interacting point particles describing cell–cell contacts within a certain interaction radius, based on [19], without modeling the cell shapes explicitly as implemented in the cellular Potts models [31] and the biochemical models [34]. Our model demonstrates that the alignment information transmitted through the cell–cell interactions, in the presence of a constant influx of cells into the channel, is sufficient to generate a directed collective migration over long distances. In this regime, we further analyze how the individual cell-level motility and channel properties (e.g., width of the channel and the influx rate of the cells into the channel) would influence the properties of the population-level motility, including the alignment of collective migration, the migration time for a cell to cross the domain, and the cell density in the domain. The results are discussed in the context of experiments and other theoretical studies.

II. MODEL DESCRIPTION

First, we run preliminary simulations using a model where the cell shapes are modeled as contours, similar to the one described in Ref. [33]. Then, based on these observations we study the same problem in more details using the simplified, but computationally more efficient particle-based model [19].

Briefly, in Ref. [33], the migration of cells was modeled in a closed square shaped domain with periodic boundaries. The shape of the cells was initialized as contours (composed of a circular core surrounded by a deformable region representing cell protrusions) in polar coordinates with a Gaussian function of the angle θ:

$$Q_0(\theta;\theta_0) = R_0 + Ae^{-(\theta-\theta_0)^2/2\omega^2}, \qquad \theta_0 - \pi < \theta < \theta_0 + \pi, \tag{1}$$

where R_0 is the radius of the cell core, A and ω are the cell shape parameters, θ_0 is the instantaneous cell orientation [33]. Numerically, the contours are approximated by a discrete set of m points, corresponding to equally distributed orientations $\theta_k = 2\pi k/m$, where $k = 1, .., m$. The cell shape function $Q_0(\theta;\theta_0)$ is then used to determine the cell velocity in the direction of net force produced by cell protrusions:

$$\vec{v}(t) = V_0 \int_0^{2\pi} (Q_0(\theta) - R_0)\vec{n}_\theta \mathrm{d}\theta, \tag{2}$$

where V_0 is a constant velocity parameter and $\vec{n}_\theta$ is the radial unit vector in the direction θ. In the absence of cell–cell interactions, a single cell moves with the velocity given by Eq. (2) with an additional random noise:

$$\frac{\mathrm{d}\vec{r}}{\mathrm{d}t} = \vec{v}(t) + \vec{\eta}(t), \qquad \langle \vec{\eta}(t)\cdot\vec{\eta}(t-\tau)\rangle = \sigma^2\delta(\tau), \tag{3}$$

where $\vec{\eta}(t)$ is an uncorrelated white noise with the intensity σ. When two cells collide, due to CIL, their protruded contours collapse and, as a result, the cells redirect their movement. In numerical simulations, overlapping protrusions are detected and in the corresponding radial directions the contours are reset to the core radius. The collapse of protrusions breaks the symmetry of the cell with respect to the original orientation axis. Due to this modified shape of the contour the cells move away from each other and gradually regain their normal shape and velocity by reforming protrusions symmetrically along the new movement direction. At each time step, the velocity vector is determined from the newly updated cell shape $Q_0(\theta;\theta_0)$ according to Eq. (2), and the orientation of the velocity vector is combined additively with the noise corresponding to Eq. (3). The resulting direction $\theta_0(t)$ determines the orientation of the target Gaussian cell shape $Q_0(\theta;\theta_0(t))$ according to

$$\frac{\partial Q(\theta,t)}{\partial t} = -\gamma[Q(\theta,t) - Q_0(\theta;\theta_0(t))] + \xi(\theta,t), \tag{4}$$

where γ is the regrowth rate of the cell contour; and for a more realistic representation of the cells here we also include a noise term ξ which describes random fluctuations of the cell protrusions, since pseudopodia are randomly distributed along the cell perimeter [41]. Note that $\theta_0(t)$ is determined by the orientation of the cell velocity vector $\vec{v}(t)$ defined by the integral in Eq. (2).

Results from preliminary simulations with this contour-based cell model are shown in Fig. 1. Starting with an empty channel with solid reflecting boundaries at the top, bottom, and left, the cells enter the channel on the left side at a constant rate with random initial direction, uniformly distributed between 0 and 2π. When a cell hits a boundary its shape changes so that the part of the protrusion that is outside of the domain

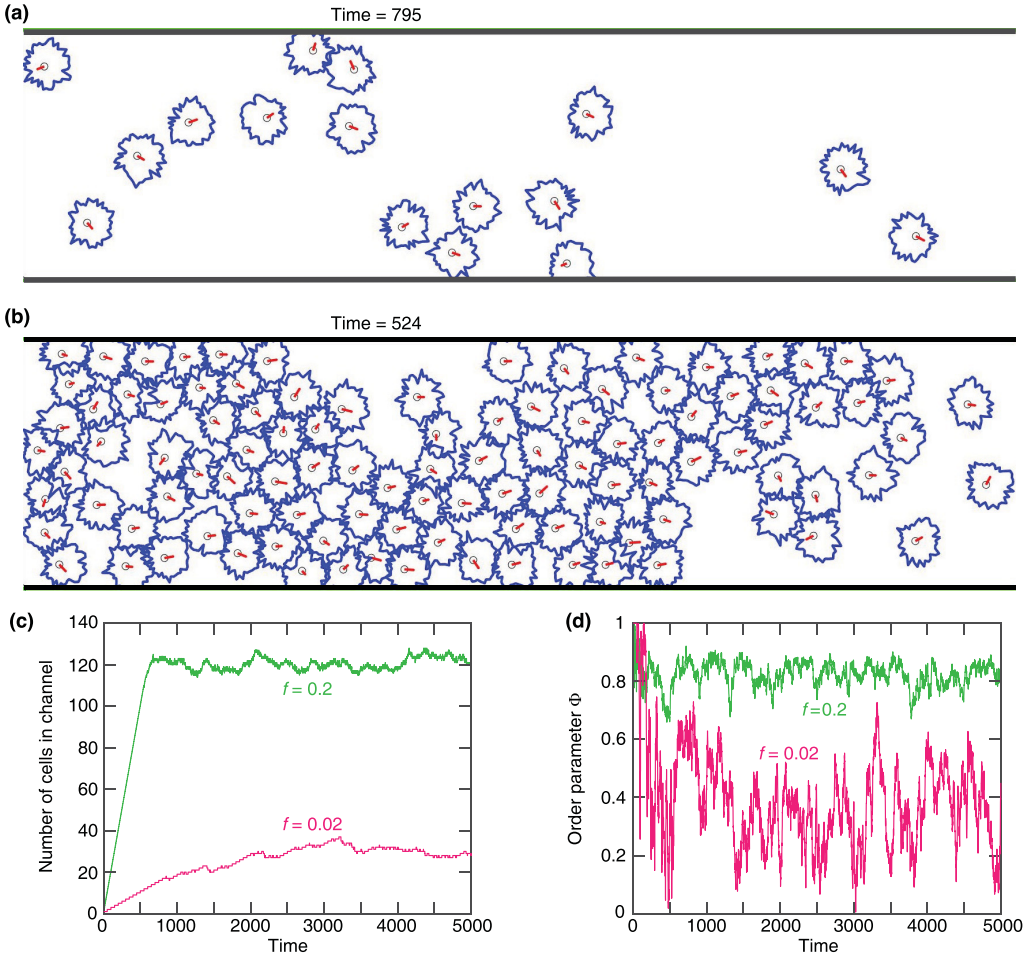

FIG. 1. Migration of cells simulated with the contour-based model. (a), (b) Snapshots of cells in an open migratory domain with a channel geometry and dimensions $L_x = 40$ and $L_y = 10$, where top and bottom boundaries are reflective. Flux rates f are 0.02 (a) and 0.2 (b). Other simulation parameters are: $R_0 = 0.5, A = 0.5, \omega = 2, V_0 = 1, \gamma = 0.5, \xi = 0.1$, and $\eta = 0.1$. For each cell shape, red arrow: the instantaneous cell velocity; black circle: cell body with radius R_0; blue contour: cell shape; see Eq. (1). (c) Simulations are run long enough to observe that the number of cells in the channel remains steady. (d) Order parameter Φ versus time. For $f = 0.2$, $\Phi = 0.83 \pm 0.04$. For $f = 0.02$, $\Phi = 0.39 \pm 0.17$.

is removed which leads to a change in the direction of movement. For simplicity, it is assumed that cells exit the channel from the right end of the channel. Therefore, when the cells reach the right end of the channel they are eliminated from the simulation. The simulations were run until the cell numbers in the channel reached an approximate steady state; see Fig. 1(c). The simulation was repeated with different values of the input cell flux into the channel. The main observation from these simulations is that when the input flux is relatively high the migration is well ordered, i.e., cells move in approximately the same direction, and when the input flux is low there is a lower cell density in the channel and the cells often loose the overall direction of the migration and follow a longer random forward-and-backward trajectory to get through the channel; see Fig. 1(d) and Movies 1 and 2 in the Supplemental Material [42]. The collective alignment of migrating cells can be characterized by the order parameter:

$$\Phi = \frac{\left|\sum_i \vec{v}_i\right|}{\sum_i |\vec{v}_i|}, \tag{5}$$

where Φ varies between 0 (uncorrelated random movement) and 1 (fully aligned migration). The order parameter as a function of time for two values of the input flux is shown in Fig. 1(c).

In order to characterize the properties and more detailed parameter dependence of the cell migration in the open channel, we use a simplified particle-based computational model. We have shown earlier [33] that in a closed domain the contour-based cell model has similar properties and produces qualitatively similar phases of ordered coherent and irregular movement as the self-propelled particle-based model introduced in Ref. [19]. The effective alignment interaction of the Vicsek model [19] was found to also arise from various other types of cell–cell interactions [43–48]. Therefore, we model the migratory properties using the particle-based cells in an open domain.

We assume that the self-propelled cells (particles) enter the domain on the left side of the channel at a fixed rate f, defined as the number of new cells added per unit time (see Movie 3 and 4 [42]). The model is discrete in time so the time step taken to update the cell positions is the time unit, $\Delta t = 1$.

Following [19], each cell i moves in the domain by updating its position $\vec{r}_i = (x_i, y_i)$ at each time step as

$$\vec{r}_i(t+1) = \vec{r}_i(t) + \vec{v}_i(t)\Delta t \tag{6}$$

with a constant velocity of magnitude v_0:

$$\vec{v}_i(t) = v_0\vec{n}_i. \tag{7}$$

To determine the direction of the self-propelling particles that interact, in a well-known model Vicsek and colleagues used the average velocity direction of the neighboring particles [19]. Without considering information about the movement directions of neighbors, the collective direction can be determined by assuming only short-range interactions [49]. This later experimentally motivated model exhibited a continuous phase transition from a disordered into an ordered state, which indeed belongs to the same universality class as the model in Ref. [19]. Therefore, following the fundamental model in Ref. [19], here, the direction of the displacement $\vec{n}_i = (\cos\alpha_i, \sin\alpha_i)$ is calculated as

$$\alpha_i(t) = \langle\alpha_j(t)\rangle_R + \Delta\alpha, \tag{8}$$

where $\langle\alpha_i(t)\rangle_R$ is the average of the velocity directions α_j of the cells (including cell i) within an interaction circle of radius R surrounding cell i. $\Delta\alpha$ is a random noise term uniformly distributed over the interval $[-\eta/2, \eta/2]$ [19]. When a cell hits the top or bottom boundary, the orientation of the particle is reflected as $\alpha_i \to 2\pi - \alpha_i$. We also used reflecting boundary conditions on the left end of the domain by changing the orientation of the particles when they cross $x = 0$ as $\alpha_i \to \pi - \alpha_i$. Finally, when a cell reaches the right end of the channel, it is removed from the simulation, resembling a target region where neural crest cells stop migrating and differentiate into various cell types [29,50].

Since the cells are moving in an open domain, the cell density ρ is not prescribed as in the closed system studied earlier [19,33], and is determined by the influx rate of the cells. By simplifying the cell shapes into a single cell–cell interaction radius, the number of free parameters is reduced, having only the flux parameter f in addition to the three cell parameters v_0, η, and R. We will choose the interaction distance as the length scale unit in the particle based simulations, i.e., $R = 1$.

Using the simulations based on Eqs. (6)–(8), we focus on three characteristics of the collective migration: the alignment of migration calculated using the order parameter defined in Eq. (5), the migration time, and the cell density in the domain. The migration time t_m for a cell is defined as the time taken for crossing the channel from left to right. Finally, the cell density ρ is calculated by binning the domain along the x dimension, where the width of each bin is five length units. The cell density ρ is then calculated as the average number of cells located in each bin divided by the area of the bin.

III. RESULTS AND DISCUSSION

We first examine how the properties of the migratory dynamics Φ, ρ and t_m change in response to the influx rate f of the cells into the domain. Typical snapshots of the cell distribution in the channel in the stationary regime, are shown in Figs. 2(a)–2(c). We find that increasing the flux rate f promotes the migration alignment, accelerates the average migration time, and increases the cell density in the domain; see Figs. 2(d)–2(f). The distribution of the migration times also shows that at lower input flux, in addition to the increased average migration time, the variability of the time needed to cross the channel also increases [see the broadening of the distributions in Fig. 2(f)] indicating the increased randomness of the individual cell trajectories.

For comparison, we also simulated the migration in the case when the interaction between the particles was switched off, i.e., the interaction radius R was set to zero (Fig. 3). In this case, the cells follow discrete random-walk trajectories, with step-size v_0 and random direction $\alpha_i(t+1) = \alpha_i(t) + \Delta\alpha$. In the absence of interactions, the particles have no information about the direction of migration. This leads to a highly nonuniform distribution along the channel with more cells accumulating on the left side of the domain where they enter the channel; see Figs. 3(a) and 3(c). The stationary density distribution along the channel can be described by a one-dimensional diffusion equation with constant flux (f) boundary condition on the left, and zero density on the right:

$$\frac{\partial\rho(x,t)}{\partial t} = D\frac{\partial^2}{\partial x^2}\rho(x,t), \quad -D\frac{\partial}{\partial x}\rho|_{x=0} = f,$$
$$\rho(x = L_x, t) = 0, \tag{9}$$

where D is the diffusion coefficient of the cells. The stationary solution of the diffusion Eq. (9) corresponds to a constant density gradient $\rho(x) = (L_x - x)f/D$ which agrees with the numerical simulations shown in Fig. 3(c). Therefore, results in Fig. 3 demonstrate that in the absence of alignment interactions (i.e., without CIL) the influx of cells is not sufficient in itself to generate a directed collective migration.

We also examine the migratory dynamics when cells move with the maximum noise intensity (i.e., $\eta = 2\pi$). The model predicts a nonuniform distribution of particles along the channel, similar to the diffusive behavior found for the noninteracting cells with a lower η; see Fig. 3(c). Likewise, the order parameter reduces to $\Phi \approx 0.1$, confirming the role of the directional interactions in aligning a collective migration; Fig. 3(b). In this diffusive regime, the cell density is higher on the entry side of the channel resulting in an increase in the migration time; see Fig. 3(d).

With increasing flux rate f, the random movement of cells changes to organized collective migration, where the migration alignment is maximised and the migration time is minimized; see Figs. 4(a) and 4(b). A similar transition from a sparse domain into a dense one is also obtained with increasing f; see Fig. 4(c).

These results motivate us to test the effect of the input flux rate on another cell mobility characteristic: the directional persistence of the cell's displacement trajectories. The persistence length P of cell trajectories determines how far cells can migrate within the channel in a given amount of time, and is determined by fitting the following equation:

$$\langle R^2\rangle = 2P^2\left(\frac{L}{P} - 1 + e^{-\frac{L}{P}}\right), \tag{10}$$

to the mean squared displacement $\langle R^2\rangle$ of the trajectories of length L [51–53]. We explore the persistence length P versus the input flux f with varying the noise intensity η. First, we

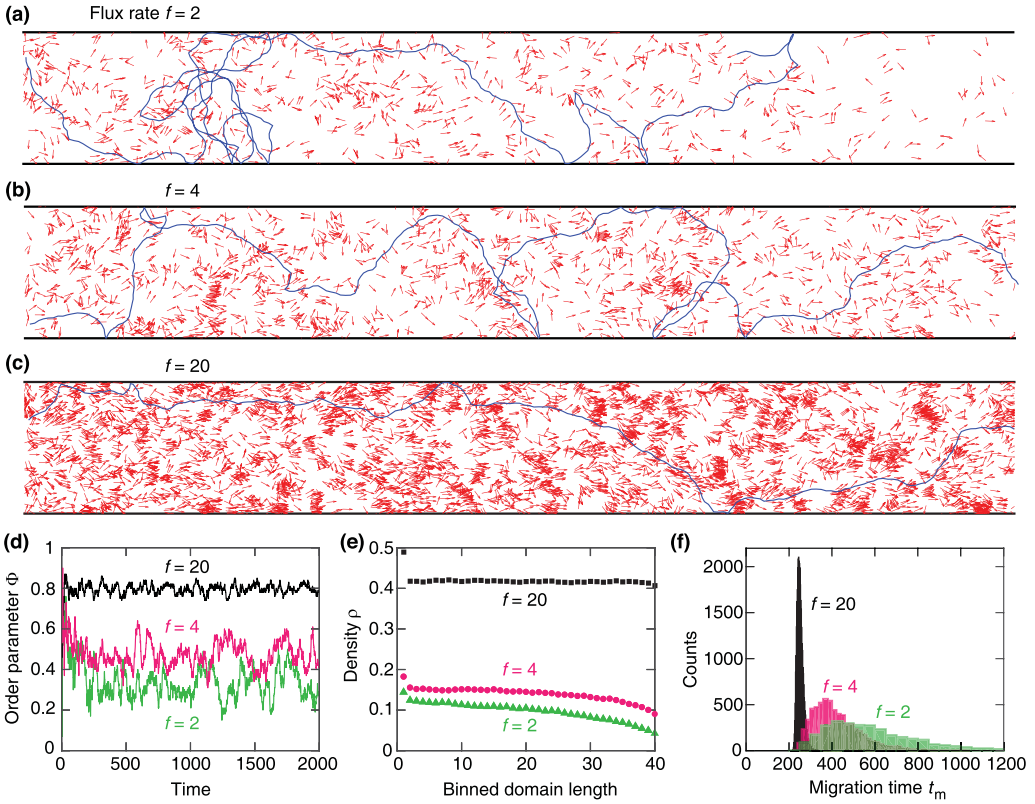

FIG. 2. Migratory dynamics simulations of the particle model. (a)–(c) Snapshots of cells, modelled as self-propelled particles, in an open channel with dimensions $L_x = 400$ and $L_y = 60$, where the top and bottom boundaries are reflective. Flux rates are 2 (a), 4(b), and 20 (c) at time 500. Other simulation parameters are $v_0 = 2$, $\eta = 1$, and $R = 1$. Each red arrow: velocity of a cell. Blue trajectory: displacement trajectory of a cell randomly selected at the start of the simulation. (d) Order parameter Φ versus time. For $f = 2$, $\Phi = 0.34 \pm 0.09$. For $f = 4$, $\Phi = 0.48 \pm 0.07$. For $f = 20$, $\Phi = 0.80 \pm 0.03$. Parameter values correspond to mean $\pm$ standard deviation (SD). (e) Cell density ρ versus the binned length of the domain, where each bin is five length-unit wide. ρ are 0.19 ± 0.05, 0.28 ± 0.03, and 0.84 ± 0.02 for flux rates $f = 2$, 4, and 10, respectively. (f) Distribution of the migration time t_m needed for cells cross the domain. For $f = 2$, $t_m = 587.07 \pm 219.34$. For $f = 4$, $t_m = 419.76 \pm 111.19$. For $f = 20$, $t_m = 251.14 \pm 14.94$.

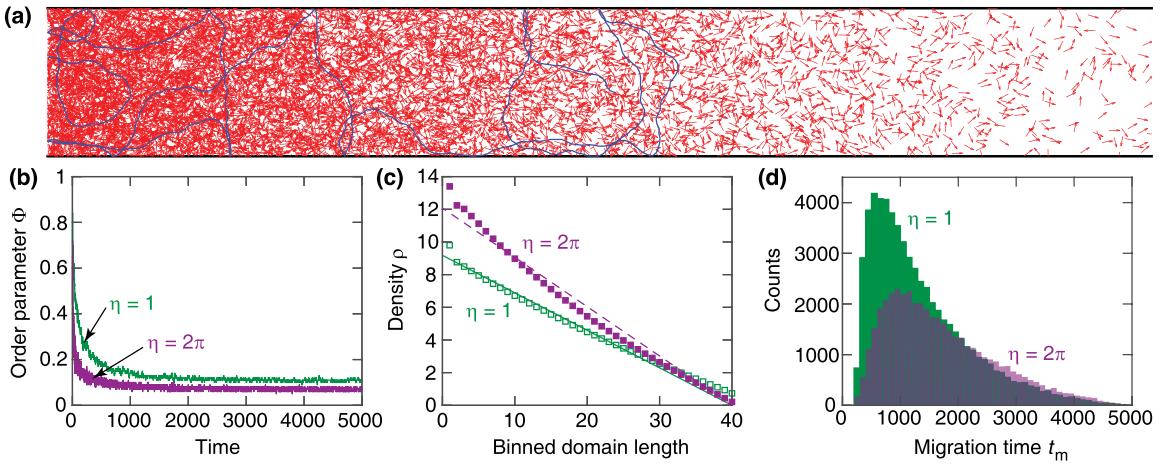

FIG. 3. Migratory dynamics of noninteracting particles (i.e., $R = 0$) with the maximum noise intensity (i.e., $\eta = 2\pi$). (a) A snapshot of noninteracting particles in an open domain with dimensions $L_x = 400$ and $L_y = 60$ at time 500. Simulation parameters are $f = 20$, $v_0 = 2$, and $\eta = 1$. Each red arrow: velocity of a cell. Blue trajectory: displacement trajectory of a cell randomly selected at the start of the simulations. (b) The order parameter Φ is equal to 0.14 ± 0.07 (for $\eta = 1$) and 0.08 ± 0.04 (for $\eta = 2\pi$). (c) Cell density ρ versus the binned length of the domain, where each bin is five length-unit wide. Lines: fit of $\rho(x) = (L_x - x)m$, where the slope m, which is equal to 0.14 ± 0.01 (for $\eta = 1$) and 0.22 ± 0.01 (for $\eta = 2\pi$), corresponds to f/D; see Eq. (9). Least-squares fitting was performed using MATLAB (version 2017b, The MathWorks, Inc.). (d) The migration time t_m is equal to 1338.35 ± 847.16 (for $\eta = 1$) and 1702.28 ± 933.48 (for $\eta = 2\pi$).

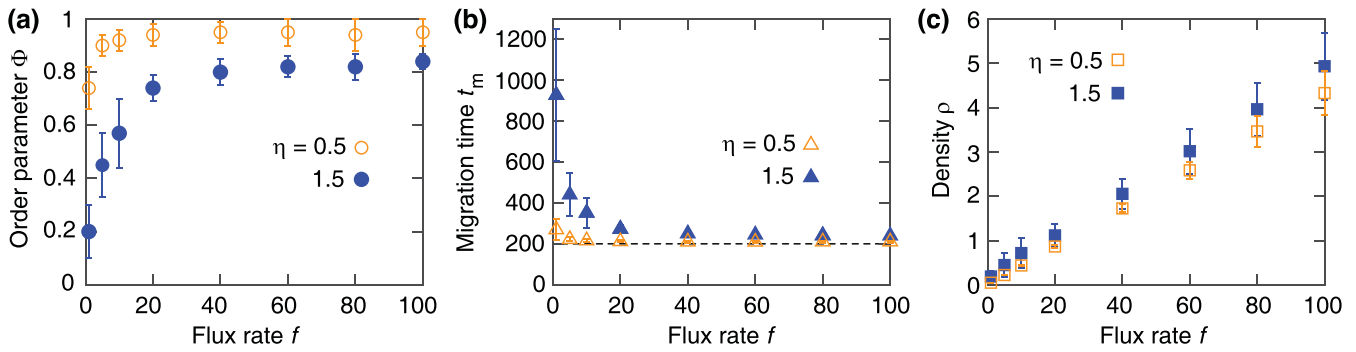

FIG. 4. Migratory dynamics of cells versus the influx rate f, obtained using the particle model. Order parameter Φ (a), migration time t_m (b), and cell density ρ (c) calculated with model parameters $v_0 = 1$ and $R = 1$ for $\eta = 0.5$ and 1.5. Open domain dimensions: $L_x = 400$ and $L_y = 60$. Dashed line in (b): minimum migration time L_x/v_0.

calculate the mean square of the end-to-end distance R of the particle trajectories of various lengths L generated from the simulations; see symbols in Fig. 5(a). Then, fitting Eq. (10) to the $\langle R^2 \rangle$ versus L calculations estimates P; see curves in Fig. 5(a). We find that the persistence length of migrating cells

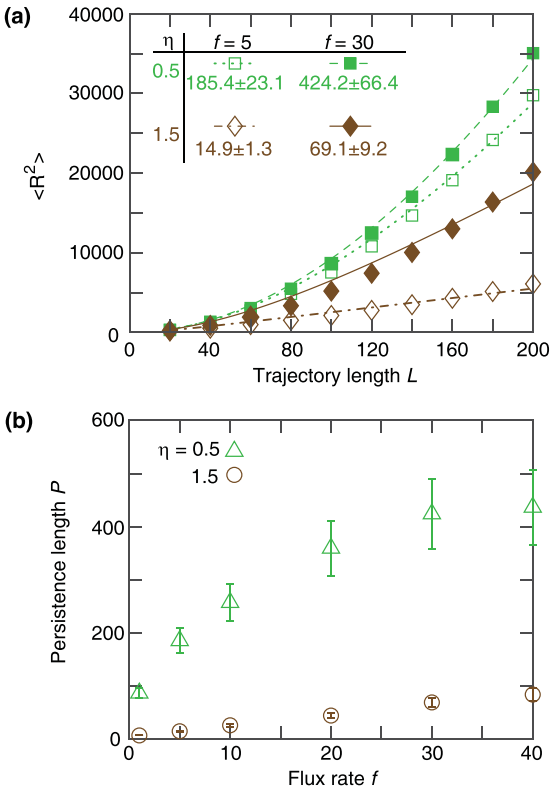

FIG. 5. Persistence length of the migrating cells calculated using the particle model. (a) Four example calculations of the mean square of the end-to-end distance R of the displacement trajectories of particle versus the trajectory length L. Symbols: $\langle R^2 \rangle$ of trajectories generated from the particle model simulations. Curves: fit of Eq. (10) to the symbols, performed using MATLAB (version 2017b, The MathWorks, Inc.). Inset: the persistence length P values correspond to mean ± standard error (SE). (b) The persistence length P versus the influx rate f (mean ± SE). Simulation parameters $v_0 = 1$ and $R = 1$ for $\eta = 0.5$ and 1.5 with an open domain of dimensions $L_x = 400$ and $L_y = 60$.

increases with the input flux. It is also found that the noise intensity lowers the persistence length; see Fig. 5(b).

We further examine how the migratory characteristics change depending on the cell's parameters. In addition, we analyze the effect of the width of the domain L_y on these characteristics, since earlier studies have shown that a spatial confinement [31] and growing domain [25,36] may affect the collective migration of cells.

The cell velocity parameter v_0 is found to have no significant effect on the migration alignment, but increasing v_0 lowers the migration time and cell density, as shown in Figs. 6(a)–6(c). Using a continuum representation of the moving cells, we can describe the flux in the channel as the product of the average velocity and density. The average local velocity of cells can be written as the product of the individual cell velocity (v_0) and the order parameter Φ. In a stationary state, when the average density is approximately constant in time, the flux inside the channel is balanced by the input flux of cells entering the channel leading to the relationship:

$$f = v_0 \Phi \rho. \tag{11}$$

The validity of this relationship, in the form of $\rho(v_0) = (f/\Phi)v_0^{-1}$ is shown in Fig. 6(c).

Thus, in the open channel the stationary cell density is determined by the input flux through the following feedback mechanism: increasing the input flux f leads to higher density, which produces more ordered alignment of the cells' movement. This is a consequence of the relationship between the density and order parameter already well established in closed domain with constant prescribed density [19,33]. The increased order parameter raises the flux of cells through the channel and reduces the density, thus producing a negative feedback and a stable equilibrium density.

The analysis of the stochasticity of the cells movement indicates that increasing the noise intensity η can transition a coordinated migration to a random movement of cells. The randomness in the movement of the cells blocks their coordination in migrating as a collective. In turn, this leads to an increased cell density in the domain; see Figs. 6(d)–6(f).

Finally, we find that the collective migration becomes more aligned and faster with narrowing the domain; see Figs. 6(g)–6(i). A narrow domain increases the chance of cell collisions, suggesting that spatial confinement strengthens the effect of CIL in coordinating the collective migration. For example,

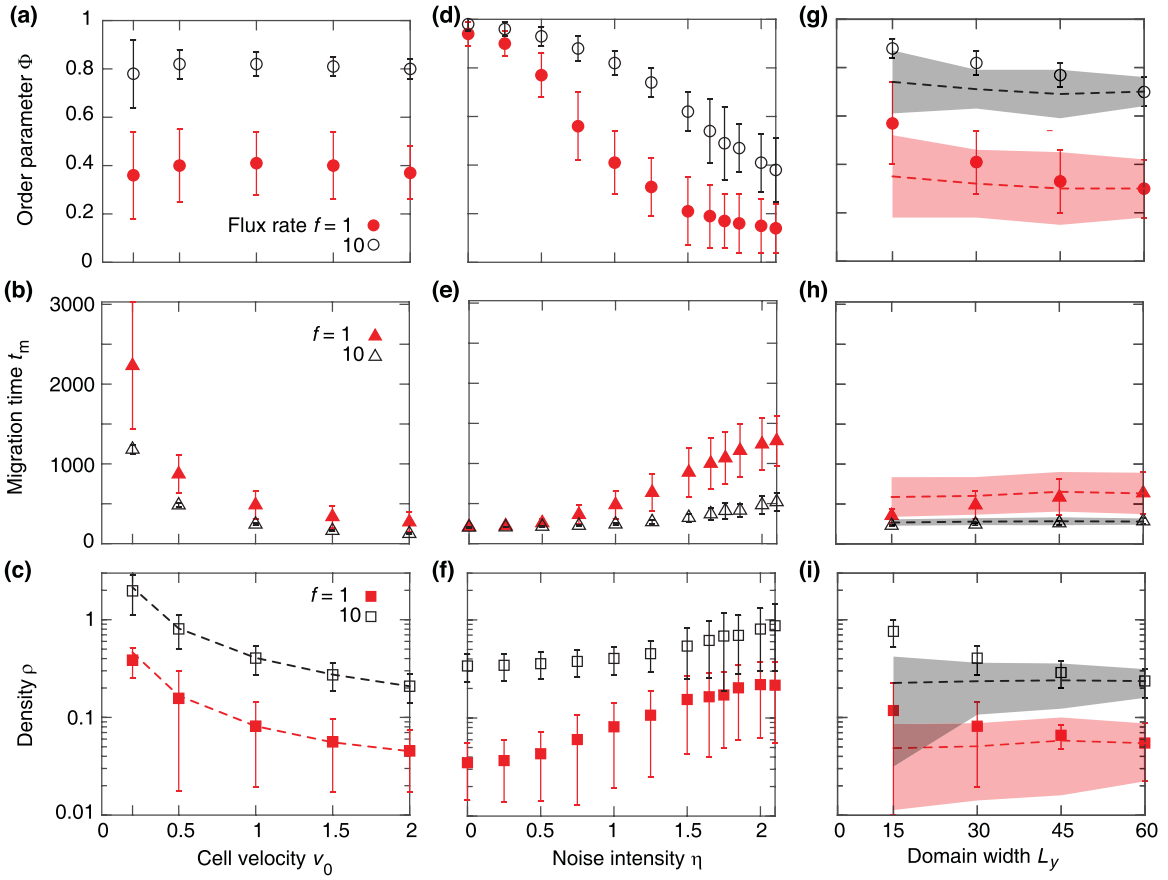

FIG. 6. Migratory dynamics of cells calculated using the particle model. Order parameter Φ (top row), migration time t_m (middle row), and cell density ρ (bottom row) versus cell velocity v_0 (a)–(c), noise intensity of the cell motility η (d)–(f), and width of the open domain L_y (g)–(i). $L_x = 200$. In (a)–(f), $L_y = 60$. In (\textrma)–(c), $\eta = 1$ and $R = 1$. Dashed curves in (c) calculated as $f/(v_0\Phi)$ normalized to L_y. In (d)–(f), $v_0 = 1$ and $R = 1$. In (g)–(i), $v_0 = 1$, $\eta = 1$, and $R = 1$. Dashed curves: mean Φ, t_m, and ρ versus L_y for different flux density values, proportional to L_y. Shaded region: SD. For example, with $f = 1$ and $L_y = 15$, one cell enters the domain every four time steps.

the order parameter decreases with the domain width; see Fig. 6(g). Narrowing the domain (at fixed f, v_0, η, and R) accelerates the cell collision rate, resulting in a faster convergence of the displacement directions α_i to an aligned direction. Accordingly, enhancing f, would increase Φ. When the input flux f is proportional to the width of the domain (e.g., for $f = 1$ with $L_y = 30$, one cell enters the domain every second time-step), negligible changes in Φ, t_m, and ρ are found; see dashed curves in Figs. 6(g)–6(i).

To represent the relationship between the average cell density ρ and the order parameter Φ in an open domain, we can eliminate the flux parameter f in the calculations of $\rho(f)$ and $\Phi(f)$ in Figs. 4(a)–4(c). The result of this is shown in Fig. 7(a). Higher cell density, which is produced by increased incoming flux of cells, leads to a more coordinated ordered migration. We can now compare this result to the closed system where there is no flux across the domain and the cell density is an externally controlled parameter determined by the initial condition. We find the same transition from disordered to ordered collective movement in response to the cell density ρ; see Fig. 7(b). We further explore this relationship between ρ and Φ with the contour-based model. While the order parameter and density both increase with the input flux, similarly to the particle model, the cell density in the channel saturates at a maximum value; see Figs. 8(a) and 8(b). This illustrates the effect of the volume exclusion (i.e., a cell cannot occupy space that is already occupied by another cell [54]) in the contour-based model, which is absent in the particle model; compare Figs. 4(c) and 8(b). However, the maximum density is reached at flux values when the system is already in the ordered migration regime, therefore volume exclusion does not affect the relationship between ρ and Φ.

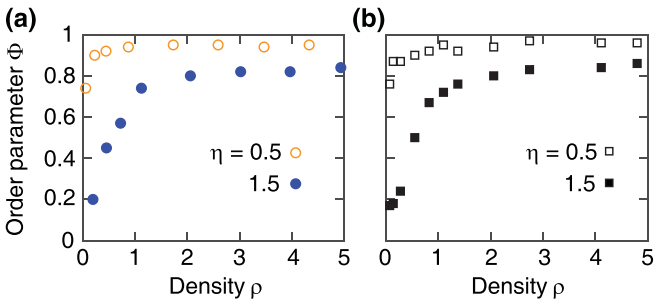

FIG. 7. Alignment of collective migration versus the cell density calculated using the particle model in (a) open (400 × 60) and (b) closed (60 × 60) domains. Simulation parameters are $v_0 = 1$ and $R = 1$ for $\eta = 0.5$, and 1.5.

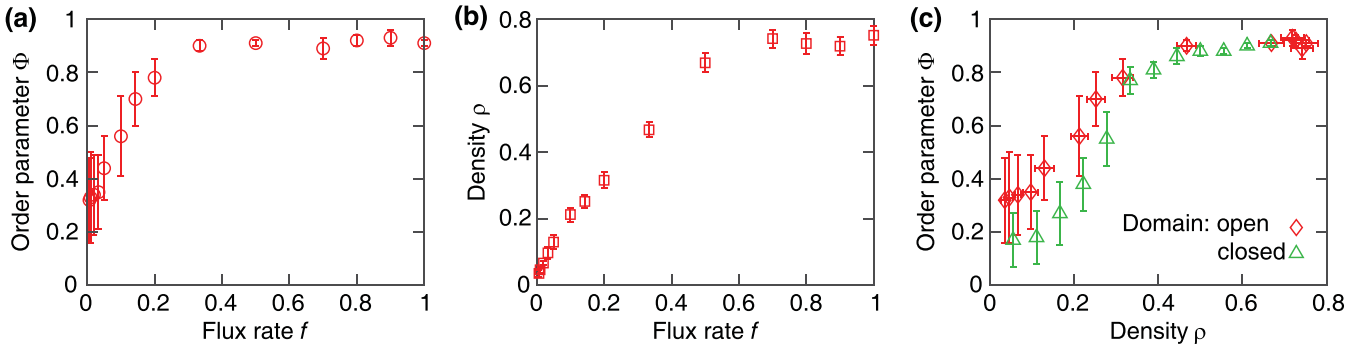

FIG. 8. The alignment of collective migration versus the cell density calculated using contour-based model in open (40 × 10) and closed (30 × 30) domains. Simulation parameters: $R_0 = 0.5$, $A = 0.5$, $\omega = 2$, $V_0 = 1$, $\gamma = 0.1$, $\xi = 0.1$, and $\eta = 0.05$.

We again find a consistent transition from disordered to ordered migration in the ρ versus Φ relation obtained from the contour-based cell model with both open and closed domains; see Fig. 8(c). These agreements show that the simplified particle model can reproduce the results of the more complex contour-based model in Ref. [33]; see Movies 3–5 [42].

Our results are in agreement with experimental and earlier theoretical findings. Experiments have shown that CIL dramatically increases the percentage of the neural crest cells that reach their target region over time [29,31]. Likewise, Woods *et al.* [30] found that the cell–cell interactions reduce the time taken for the cells to reach a target location. These observations confirm our results on the migration alignment and time in Figs. 2(d) and 2(f), which are further analyzed versus the motility properties of the cells.

The analysis of the effect of the randomness in the movement of the neural crest cells in Figs. 6(d)–6(f) has shown that stochastic fluctuations in the movement of cells limit the coordination of the migration. This agrees with our earlier results in Ref. [33], and the flocking models (where the self-propelled particles had nonlocal interactions) [19,49], the self-propelled short-range interacting agents in swarm migration [55], and the self-propelled interacting cells [56] that the amplitude of the stochasticity of the movement of cells leads to random movement.

In addition, previous experimental and theoretical studies on the effect of the spatial confinements on the migration of neural crest cells have shown that removing the lateral confinement of the domain significantly reduces the directionality of the collective movement [31,34]. In agreement with these findings, the model calculated higher order parameter Φ for narrower domains; see Fig. 6(g).

Finally, experiments have shown that the CIL interaction of neural crest cells during migration increases migratory persistence (i.e., the maximum distance along a cell trajectory divided by the total length of that trajectory) [31]. Moreover, the self-propelled particle models have indicated that the particle density transitions particles' random movement to a coordinated migration [49,55]. Together, this implies that the coordination of the migration would increase in response to an increase in the cell density in the domain. This has been shown in our calculations for the flux-dependent persistence length in Fig. 5(b) and the density-dependent order parameter in Figs. 7(a) and 7(b).

IV. CONCLUSION

We extended our computational model of the analysis of the migration of the neural crest cells [33] to an open domain. This allowed us to take into account the effect of the flux rate of the cells into the domain on the migration alignment and cell density, in the absence of proliferation and chemoattraction. Our results suggest that when there is a sufficiently strong sustained flux of cells into a confined channel the cells interacting via CIL alone can maintain persistent directed migration without directional chemotactic signals; see Figs. 2(a)–2(c) and 3(a), blue trajectories. This resembles the observations in Ref. [37], where the role of lead and trailer neural crest cell identities examined that trailer neural crest cells do not require chemotactic signaling factor (vascular endothelial derived growth) for guidance, but instead receive guidance instructions from lead cells. The alignment of the directed migration is determined by the cell density the same way as in a closed system of interacting self-propelled particles [19] or contour-based cells [33]. While in a closed system with periodic boundary conditions there are multiple choices for the common direction, in the open channel a single direction consistent with the domain boundaries is selected. Previous modeling work has shown [34] that directed collective migration of cell clusters is possible when there is coattraction between the cells mediated by a diffusing chemical signal. Our model demonstrates that the key factor for collective coherent movement is the cell density, and therefore the coattraction mechanism is not necessary when the cell density is maintained by a continuous flux of cells entering the channel. In this case, the density is determined by the balance between the external flux f and the flux in the channel defined by $v_0\rho\Phi(\rho)$.

Data availability

The computer code is available to download from the website [57]. The code has been developed using MATLAB version R2017b, The MathWorks, Inc.

ACKNOWLEDGMENTS

A.C. was supported by the NIH (Grant No. DE026172) and the Hungarian National Research, Development and Innovation Office (Grant No. 132225). Z.N. was supported by ARC Discovery Project No. DP160104342.

[1] A. Szabó and R. Mayor, Mechanisms of neural crest migration, Annu. Rev. Genet. **52**, 43 (2018).

[2] M. Simoes-Costa and M. E. Bronner, Establishing neural crest identity: A gene regulatory recipe, Development **142**, 242 (2015).

[3] C. Kalcheim, The Neural Crest: A Remarkable Model System for Studying Development and Disease, in *Neural crest cells: Methods and protocols*, Methods in Molecular Biology (Springer, New York, 2019), Chap. 1, pp. 1–20.

[4] Q. Schwarz, C. H. Maden, J. M. Vieira, and C. Ruhrberg, Neuropilin 1 signaling guides neural crest cells to coordinate pathway choice with cell specification, Proc. Natl. Acad. Sci. USA **106**, 6164 (2009).

[5] S. Bhatt, R. Diaz, and P. A. Trainor, Signals and switches in mammalian neural crest cell differentiation, Cold Spring Harb. Perspect. Biol., **5**, a008326 (2013).

[6] P. M. Kulesa and R. McLennan, Neural crest migration: Trailblazing ahead, F1000Prime Rep. **7**, 10.12703/P7-02 (2015).

[7] C. Carmona-Fontaine, H. K. Matthews, S. Kuriyama, M. Moreno, G. A. Dunn, M. Parsons, C. D. Stern, and R. Mayor, Contact inhibition of locomotion in vivo controls neural crest directional migration, Nature (London) **456**, 957 (2008).

[8] P. M. Kulesa and S. E. Fraser, In ovo time-lapse analysis of chick hindbrain neural crest cell migration shows cell interactions during migration to the branchial arches, Development **127**, 1161 (2000).

[9] R. Mayor and C. Carmona-Fontaine, Keeping in touch with contact inhibition of locomotion, Trends Cell Biol. **20**, 319 (2010).

[10] J. M. Teddy, In vivo evidence for short- and long-range cell communication in cranial neural crest cells, Development **131**, 6141 (2004).

[11] E. Theveneau, L. Marchant, S. Kuriyama, M. Gull, B. Moepps, M. Parsons, and R. Mayor, Collective chemotaxis requires contact-dependent cell polarity, Dev. Cell **19**, 39 (2010).

[12] E. Theveneau and C. Linker, Leaders in collective migration: Are front cells really endowed with a particular set of skills? F1000 Res. **6**, 1899 (2017).

[13] M. Abercrombie and J. E. M. Heaysman, Observations on the social behaviour of cells in tissue culture: I. speed of movement of chick heart fibroblasts in relation to their mutual contacts, Exp. Cell Res. **5**, 111 (1953).

[14] A. Shellard and R. Mayor, Integrating chemical and mechanical signals in neural crest cell migration, Curr. Opin. Genet. Dev. **57**, 16 (2019).

[15] D. Ellison, A. Mugler, M. D. Brennan, S. H. Lee, R. J. Huebner, E. R. Shamir, L. A. Woo, J. Kim, P. Amar, I. Nemenman, A. J. Ewald, and A. Levchenko, Cell–cell communication enhances the capacity of cell ensembles to sense shallow gradients during morphogenesis, Proc. Natl. Acad. Sci. USA **113**, E679 (2016).

[16] G. Malet-Engra, W. Yu, A. Oldani, J. Rey-Barroso, N. S. Gov, G. Scita, and L. Dupré, Collective cell motility promotes chemotactic prowess and resistance to chemorepulsion, Curr. Biol. **25**, 242 (2015).

[17] E. Theveneau and R. Mayor, Integrating chemotaxis and contact-inhibition during collective cell migration: Small GTPases at work, Small GTPases **1**, 113 (2010).

[18] T. S. Deisboeck and I. D. Couzin, Collective behavior in cancer cell populations, BioEssays **31**, 190 (2009).

[19] T. Vicsek, A. Czirók, E. Ben-Jacob, I. Cohen, and O. Shochet, Novel Type of Phase Transition in a System of Self-Driven Particles, Phys. Rev. Lett. **75**, 1226 (1995).

[20] L. J. Schumacher, P. M. Kulesa, R. McLennan, R. E. Baker, and P. K. Maini, Multidisciplinary approaches to understanding collective cell migration in developmental biology, Open Biol. **6**, 160056 (2016).

[21] I. D. Couzin, J. Krause, R. James, G. D. Ruxton, and N. R. Franks, Collective memory and spatial sorting in animal groups, J. Theor. Biol. **218**, 1 (2002).

[22] I. D. Couzin, J. Krause, N. R. Franks, and S. A. Levin, Effective leadership and decision-making in animal groups on the move, Nature (London) **433**, 513 (2005).

[23] V. Guttal and I. D. Couzin, Social interactions, information use, and the evolution of collective migration, Proc. Natl. Acad. Sci. USA **107**, 16172 (2010).

[24] C. J. Torney, S. A. Levin, and I. D. Couzin, Specialization and evolutionary branching within migratory populations, Proc. Natl. Acad. Sci. USA **107**, 20394 (2010).

[25] R. McLennan, L. Dyson, K. W. Prather, J. A. Morrison, R. E. Baker, P. K. Maini, and P. M. Kulesa, Multiscale mechanisms of cell migration during development: Theory and experiment, Development **139**, 2935 (2012).

[26] M. J. Simpson, K. A. Landman, and B. D. Hughes, Multi-species simple exclusion processes, Phys. A **388**, 399 (2009).

[27] M. Bruna and S. J. Chapman, Diffusion of multiple species with excluded-volume effects, J. Chem. Phys. **137**, 204116 (2012).

[28] M. J. Simpson, D. C. Zhang, M. Mariani, K. A. Landman, and D. F. Newgreen, Cell proliferation drives neural crest cell invasion of the intestine, Dev. Biol. **302**, 553 (2007).

[29] C. Carmona-Fontaine, E. Theveneau, A. Tzekou, M. Tada, M. Woods, K. M. Page, M. Parsons, J. D. Lambris, and R. Mayor, Complement fragment c3a controls mutual cell attraction during collective cell migration, Dev. Cell **21**, 1026 (2011).

[30] M. L. Woods, C. Carmona-Fontaine, C. P. Barnes, I. D. Couzin, R. Mayor, and K. M. Page, Directional collective cell migration emerges as a property of cell interactions, PLoS ONE **9**, e104969 (2014).

[31] A. Szabó, M. Melchionda, G. Nastasi, M. L. Woods, S. Campo, R. Perris, and R. Mayor, In vivo confinement promotes collective migration of neural crest cells, J. Cell Biol. **213**, 543 (2016).

[32] K. J. Painter, J. M. Bloomfield, J. A. Sherratt, and A. Gerisch, A nonlocal model for contact attraction and repulsion in heterogeneous cell populations, Bull. Math. Biol. **77**, 1132 (2015).

[33] L. Coburn, L. Cerone, C. Torney, I. D. Couzin, and Z. Neufeld, Tactile interactions lead to coherent motion and enhanced chemotaxis of migrating cells, Phys. Biol. **10**, 046002 (2013).

[34] B. Merchant, L. Edelstein-Keshet, and J. J. Feng, A rho-gtpase based model explains spontaneous collective migration of neural crest cell clusters, Dev. Biol. **444**, S262 (2018).

[35] B. A. Camley, J. Zimmermann, H. Levine, and W.-J. Rappel, Collective signal processing in cluster chemotaxis: Roles of adaptation, amplification, and co-attraction in collective guidance, PLoS Comput. Biol. **12**, e1005008 (2016).

[36] R. McLennan, C. M. Bailey, L. J. Schumacher, J. M. Teddy, J. A. Morrison, J. C. Kasemeier-Kulesa, L. A. Wolfe, M. M. Gogol, R. E. Baker, P. K. Maini, and P. M. Kulesa,

DAN (NBL1) promotes collective neural crest migration by restraining uncontrolled invasion, J. Cell Biol. **216**, 3339 (2017).

[37] R. McLennan, L. J. Schumacher, J. A. Morrison, J. M. Teddy, D. A. Ridenour, A. C. Box, C. L. Semerad, H. Li, W. McDowell, D. Kay, P. K. Maini, R. E. Baker, and P. M. Kulesa, VEGF signals induce trailblazer cell identity that drives neural crest migration, Dev. Biol. **407**, 12 (2015).

[38] R. McLennan, J. M. Teddy, J. C. Kasemeier-Kulesa, M. H. Romine, and P. M. Kulesa, Vascular endothelial growth factor (VEGF) regulates cranial neural crest migration in vivo, Dev. Biol. **339**, 114 (2010).

[39] E. C. Olesnicky Killian, D. A. Birkholz, and K. B. Artinger, A role for chemokine signaling in neural crest cell migration and craniofacial development, Dev. Biol. **333**, 161 (2009).

[40] D. Alfandari, H. Cousin, A. Gaultier, B. G. Hoffstrom, and D. W. DeSimone, Integrin alpha5beta1 supports the migration of xenopus cranial neural crest on fibronectin, Dev. Biol. **260**, 449 (2003).

[41] S. Vedel, S. Tay, D. M. Johnston, H. Bruus, and S. R. Quake, Migration of cells in a social context, Proc. Natl. Acad. Sci. USA **110**, 129 (2013).

[42] See Supplemental Material at http://link.aps.org/supplemental/10.1103/PhysRevE.104.014405 for movies 1-5.

[43] K.-D. N. T. Lam, M. Schindler, and O. Dauchot, Self-propelled hard disks: Implicit alignment and transition to collective motion, New J. Phys. **17**, 113056 (2015).

[44] T. Hanke, C. A. Weber, and E. Frey, Understanding collective dynamics of soft active colloids by binary scattering, Phys. Rev. E **88**, 052309 (2013).

[45] S. K. Schnyder, J. J. Molina, Y. Tanaka, and R. Yamamoto, Collective motion of cells crawling on a substrate: Roles of cell shape and contact inhibition, Sci. Rep. **7**, 5163 (2017).

[46] T. Hiraiwa, Dynamic Self-Organization of Idealized Migrating Cells by Contact Communication, Phys. Rev. Lett. **125**, 268104 (2020).

[47] B. Li and S. Sun, Coherent motions in confluent cell monolayer sheets, Biophys. J. **107**, 1532 (2014).

[48] J. Löber, F. Ziebert, and I. S. Aranson, Collisions of deformable cells lead to collective migration, Sci. Rep. **5**, 9172 (2015).

[49] B. Szabó, G. J. Szöllösi, B. Gönci, Z. Jurónyi, D. Selmeczi, and T. Vicsek, Phase transition in the collective migration of tissue cells: Experiment and model, Phys. Rev. E **74**, 061908 (2006).

[50] C. E. Krull, Neural crest cells and motor axons in avians: Common and distinct migratory molecules, Cell Adhes. Migr. **4**, 631 (2010).

[51] B. M. Yeoman and P. Katira, A stochastic algorithm for accurately predicting path persistence of cells migrating in 3D matrix environments, PLoS ONE **13**, e0207216 (2018).

[52] G. Lamour, J. B. Kirkegaard, H. Li, T. P. Knowles, and J. Gsponer, Easyworm: An opensource software tool to determine the mechanical properties of worm-like chains, Source Code Biol. Med. **9**, 16 (2014).

[53] D. Selmeczi, S. Mosler, P. H. Hagedorn, N. B. Larsen, and H. Flyvbjerg, Cell motility as persistent random motion: Theories from experiments, Biophys. J. **89**, 912 (2005).

[54] R. Giniūnaitė, R. E. Baker, P. M. Kulesa, and P. K. Maini, Modelling collective cell migration: Neural crest as a model paradigm, J. Math. Biol. **80**, 481 (2020).

[55] D. Grossman, I. S. Aranson, and E. Ben Jacob, Emergence of agent swarm migration and vortex formation through inelastic collisions, New J. Phys. **10**, 023036 (2008).

[56] T. Hiraiwa, Two types of exclusion interactions for self-propelled objects and collective motion induced by their combination, Phys. Rev. E **99**, 012614 (2019).

[57] https://github.com/hr-khataee/NCCs